Detection of large-scale cloud microphysical changes and evidence for decreasing cloud brightness within a major shipping corridor after implementation of the International Maritime Organization 2020 fuel sulfur regulations

5   Michael S. Diamond

Department of Earth, Ocean and Atmospheric Science, Florida State University, Tallahassee, FL, 32306, USA

Correspondence to: Michael S. Diamond (msdiamond@fsu.edu)

Abstract. New regulations from the International Maritime Organization (IMO) limiting sulfur emissions from the shipping industry are expected to have large benefits in terms of public health but come with an undesired side effect: an acceleration

10   of global warming as the climate-cooling effects of ship pollution on marine clouds is diminished. Previous work has found a substantial decrease in the detection of ship tracks in clouds after the IMO 2020 regulations went into effect but changes in large-scale cloud properties have been more equivocal. Using a statistical technique that estimates counterfactual fields of what large-scale cloud and radiative properties within an isolated shipping corridor in the southeastern Atlantic would have been in the absence of shipping, we confidently detect a reduction in the magnitude of cloud droplet effective radius decreases

15   within the shipping corridor and find evidence for a reduction in the magnitude of cloud brightening as well. The instantaneous radiative forcing due to aerosol–cloud interactions from the IMO 2020 regulations is estimated as $O(1 \text{ W m}^{-2})$ within the shipping corridor, lending credence to global estimates of $O(0.1 \text{ W m}^{-2})$. In addition to their geophysical significance, our results also provide independent evidence for general compliance with the IMO 2020 regulations.

1 Introduction and approach

20   Since 1 January 2020, International Maritime Organization (IMO) Marine Environment Protection Committee (MEPC) regulations have limited sulfur in marine fuels from 3.5% by mass to 0.5%, or required exhaust gas cleaning systems (scrubbers) to achieve an equivalent reduction in sulfur oxide (SO_x) pollution (IMO, 2019). These IMO 2020 fuel sulfur regulations and the resulting decrease in sulfate aerosol (airborne particulate) are expected to have large benefits to public health (Partanen et al., 2013; Sofiev et al., 2018; Zhang et al., 2021). They are also expected to have an undesired side effect,

25   however: as sulfate aerosol cools the climate by reflecting sunlight directly and indirectly via changing cloud properties, the IMO 2020 SO_x reductions may accelerate global warming.

       Shipping effects on clouds were first identified in in the mid-1960s in satellite imagery of ship tracks, or curvilinear cloud perturbations following individual ships (Conover, 1966; Twomey et al., 1968). For the same amount of liquid water

within a cloud, increasing aerosol increases the cloud droplet number concentration (N_d) and decreases the effective radius
30   (r_e), brightening the clouds (Twomey, 1974, 1977). Cloud macrophysical adjustments to this aforementioned Twomey effect
have been observed within ship tracks as well, and can reinforce the microphysical brightening effect by suppressing drizzle
(Albrecht, 1989; Goren and Rosenfeld, 2012) or counteract it by enhancing entrainment (Chen et al., 2012; Coakley and Walsh,
2002; Toll et al., 2019). Challenges in understanding how much greenhouse gas warming is masked by these aerosol–cloud
interactions from shipping and other forms of pollution are the largest source of uncertainty in quantifying present-day
35   anthropogenic radiative forcing (Forster et al., 2021).

Although ship tracks have long served as "natural experiments" for testing hypotheses about aerosol–cloud
interactions in cases of clear causality (Christensen et al., 2022), until recently, attempts to observationally assess regional-to-
global-scale cloud perturbations and forcing from shipping have found negligible (Schreier et al., 2007) or null effects (Peters
et al., 2011) due to the small fraction of ships that form easily identifiable tracks and the large background variability in cloud
40   properties. New methods using machine learning have identified many times more ship tracks than has been possible with
manual identification (Watson-Parris et al., 2022; Yuan et al., 2022; Yuan et al., 2019) and analyses tracking air masses from
ship locations have shown that cloud adjustments differ systematically between easily-identifiable and "invisible" ship tracks
(Manshausen et al., 2022). Using some of these newer methods, it has been shown that ship track occurrence decreased
regionally after the introduction of emission control areas around North America and Europe and then globally after the IMO
45   2020 regulations went into effect (Gryspeerdt et al., 2019; Watson-Parris et al., 2022; Yuan et al., 2022). Large-scale changes
in cloud microphysical and macrophysical properties have been more equivocal, however. Yuan et al. (2022) found N_d
decreases within ship tracks after the IMO 2020 regulations, as expected, but, paradoxically, greater r_e decreases than before
and no difference in cloud brightness. Watson-Parris et al. (2022) did not find evidence for a change in global or regional N_d
after the IMO 2020 regulations despite the clear decrease in ship tracks, with a possible exception in the southeastern Atlantic.
50   In this work, we assess the detectability of large-scale cloud perturbations from the IMO 2020 regulations by revisiting
an alternate solution to the limitations of "bottom-up" methods tracking individual ship tracks: a "top-down" statistical
approach developed by Diamond et al. (2020), hereafter D20, to identify regional-scale cloud perturbations within a shipping
corridor in the southeastern Atlantic Ocean basin. Near-surface winds in that region blow parallel to the shipping corridor and
keep the ships' pollution constrained around the corridor, which also happens to intersect one of the world's three major
55   semipermanent subtropical stratocumulus cloud decks. D20 used a universal kriging method (Zimmerman and Stein, 2010) to
estimate counterfactual fields of cloud properties and radiation in the absence of the shipping corridor using the observed
spatial statistics of nearby, non-shipping-affected grid boxes. They found significant increases in N_d and cloud albedo (a
measure of cloud reflectivity) and decreases in r_e within the stratocumulus deck but estimated that several years' worth of data
was needed to detect a clear signal. Thus, it is possible that the effect of the IMO 2020 regulations will have just become
60   detectable using their method. Here, we apply an updated version of the D20 universal kriging algorithm to satellite retrievals
of r_e and overcast albedo (A_{cld}; top-of-atmosphere albedo when clouds are present) from the Clouds and the Earth's Radiant
Energy System (CERES) Single Scanner Footprint (SSF) product for the Terra satellite (Loeb et al., 2018; Minnis et al., 2011).

See Methods in Appendix A for details. Although Diamond et al. (2020) found a substantial decrease in cloud liquid water path within the corridor during the afternoon, no significant cloud macrophysical adjustments were found in the morning. We

65   therefore interpret any changes in r_e and A_{cld} using the Terra record (observations at ~10:30 AM local time) as being dominated by the Twomey effect. We focus on both the austral spring season (SON; September–October–November), which features the strongest shipping signal, and the annual mean (ANN), which averages a greater number of observations and thus should minimize noise. For a variable X, the "factual" or observed value in the presence of the shipping corridor is referred to as "Ship" (X_{Ship}), the counterfactual value in the absence of shipping obtained via kriging is referred to as "NoShip" (X_{NoShip}), and

70   the Ship-NoShip difference is signified as ΔX and is interpreted as the effect due to the presence of the shipping corridor.

2 Results

An unambiguous decrease in the magnitude of the r_e perturbation within the shipping corridor is evident in the 2020–2022 data as compared to the pre-2020 climatology (2002–2019) and the immediately preceding three-year period (2017–2019) during austral spring (Fig. 1). Although several significant grid boxes remain in the south of the domain (and thus some level

75   of continued shipping influence is detected), the microphysical changes are smaller and less clearly tied to the corridor; the signal is completely lost further north. Similar results are found for the annual mean values (Fig. S1), albeit with a clearer continued effect of shipping in the 2020–2022 data.

The shipping perturbation in overcast albedo is less well defined than that in the cloud microphysics, but there is still a clear perturbation in the 2002–2019 climatology and 2017–2019 data that is diminished in the 2020–2022 data in austral

80   spring (Fig. 2). Similar results are found in the annual mean, although the 2020–2022 change is more ambiguous from visual inspection alone (Fig. S2). Lower background A_{cld} values in 2020–2022, particularly in the annual mean (Fig. S2g), may be related to unusually warm sea surface temperatures (Figs. S3–4).

To assess how extreme the 2020–2022 shipping perturbation values are compared to prior three–year averages, we define a core shipping corridor region (see Methods in Appendix A) and average values over this area. To minimize effects from changing background conditions, perturbations are also calculated as relative differences (100%*ΔX/X_{Ship}). Full results

85   are reported in Table S1 and summarized in Fig. 3. For the austral spring r_e perturbations, 2020–2022 is unprecedentedly weak (Fig. 3a) and does not overlap any prior period's value within their 95% confidence intervals (Table S1). The separation between 2020–2022 and any other period's values is not as clear for austral spring A_{cld} (Fig. 3b), although the 2020–2022 perturbation values are the lowest on record and are the only period for which the effect is not distinguishable from zero at the

90   95% confidence level (Table S1). For the annual mean r_e perturbations, the 2020–2022 values are lower than any other period and the difference with the climatological value is much larger than for any other period, although the separation is not as clear as for austral spring (Fig. 3c). While the annual mean A_{cld} values for 2020–2022 are also the lowest on record, the difference from climatology is not extreme compared to other periods (Fig. 3d).

To assess whether a reduction in the shipping effect after the IMO 2020 regulations went into effect is detected at various possible levels of confidence, Table S2 reports different percentiles of the ratio of the 2020–2022 relative differences over the climatology. A decrease in the r_e perturbation is detected at greater than 99% confidence in the austral spring and at greater than 95% confidence in the annual mean, whereas decreases in the A_{cld} perturbation are only significant at the 90% confidence level in the austral spring and within the interquartile range in the annual mean. We thus conclude that the effect of the IMO 2020 regulations has been clearly detected in the large-scale cloud microphysics and that there is strong evidence for a decrease in cloud brightness, although more years of data may be required for unequivocal detection of changes in overcast albedo.

95

100
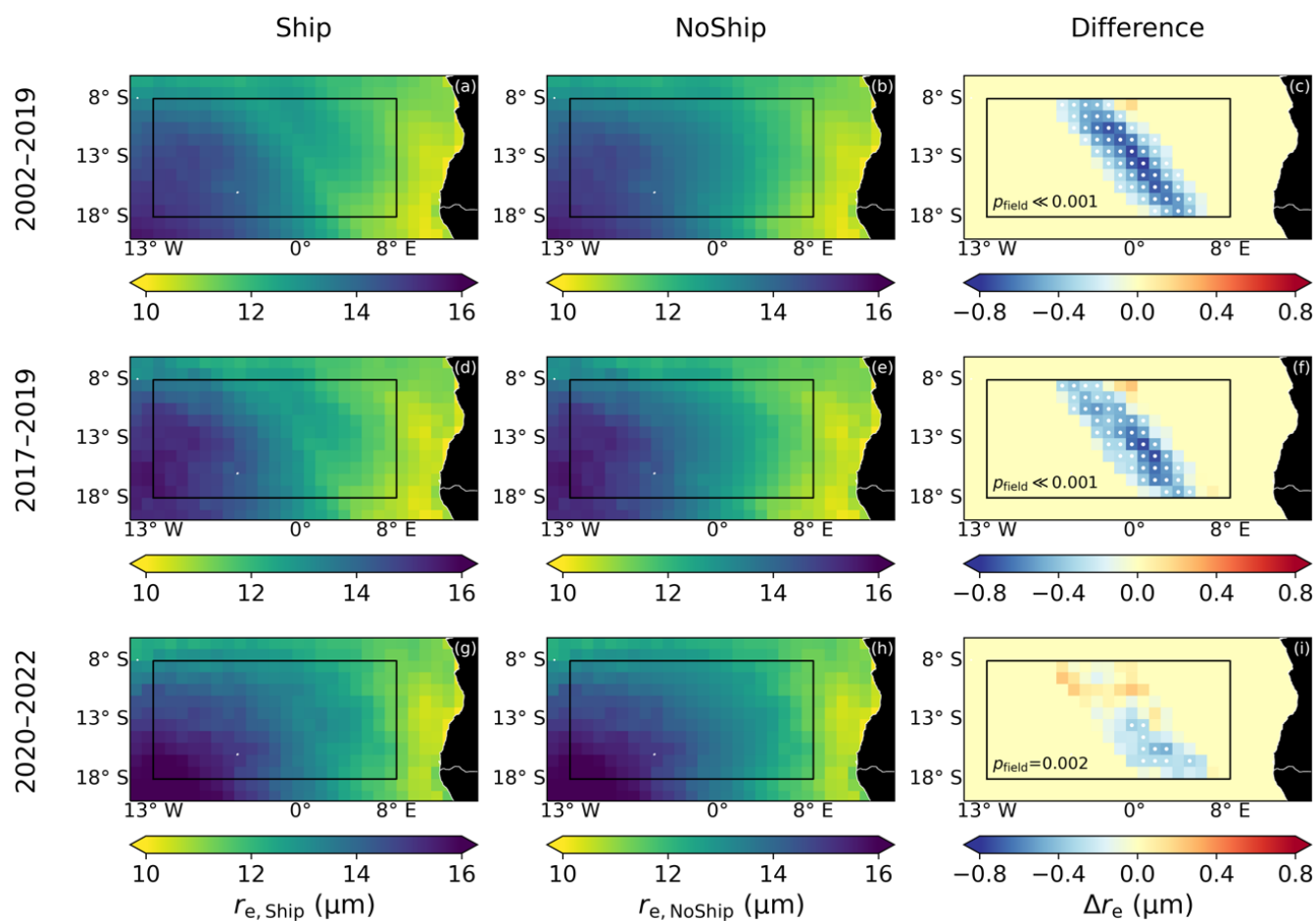
Figure 1. Maps of factual (Ship), counterfactual (NoShip), and difference (Ship-NoShip) values for austral spring liquid cloud droplet effective radius for the pre-2020 climatology (a–c), 2017–2019 (d–f), and 2020–2022 (g–i). The analysis domain of 18° S to 8° S, 13° W to 8° E is outlined in black. Grid points for which the observed values fall outside the 95% confidence interval obtained via kriging are indicated by white dots and the corresponding field significance values (p_{field}) are reported in (c,f,i).
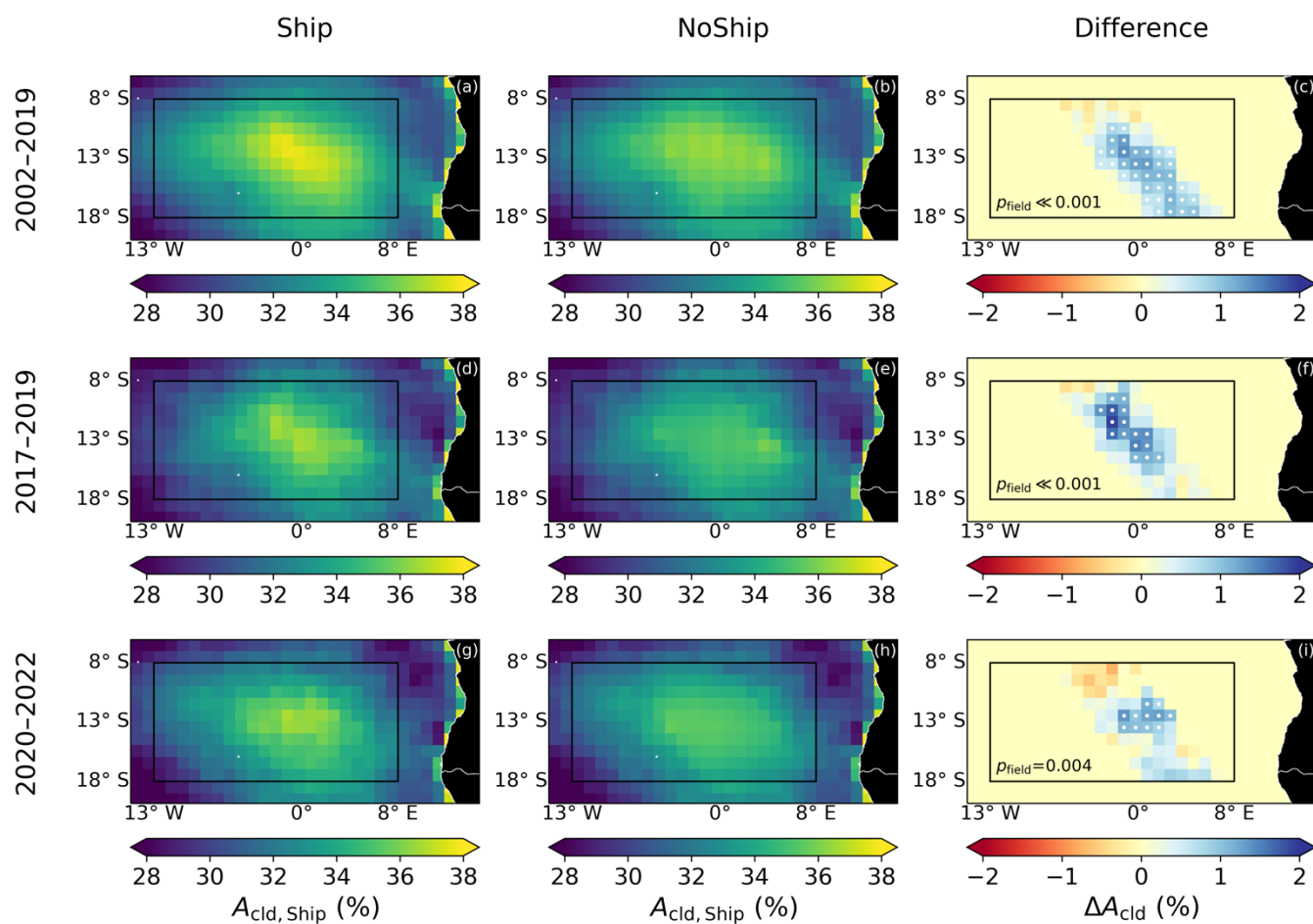
Figure 2. As in Fig. 1, but for austral spring overcast albedo.
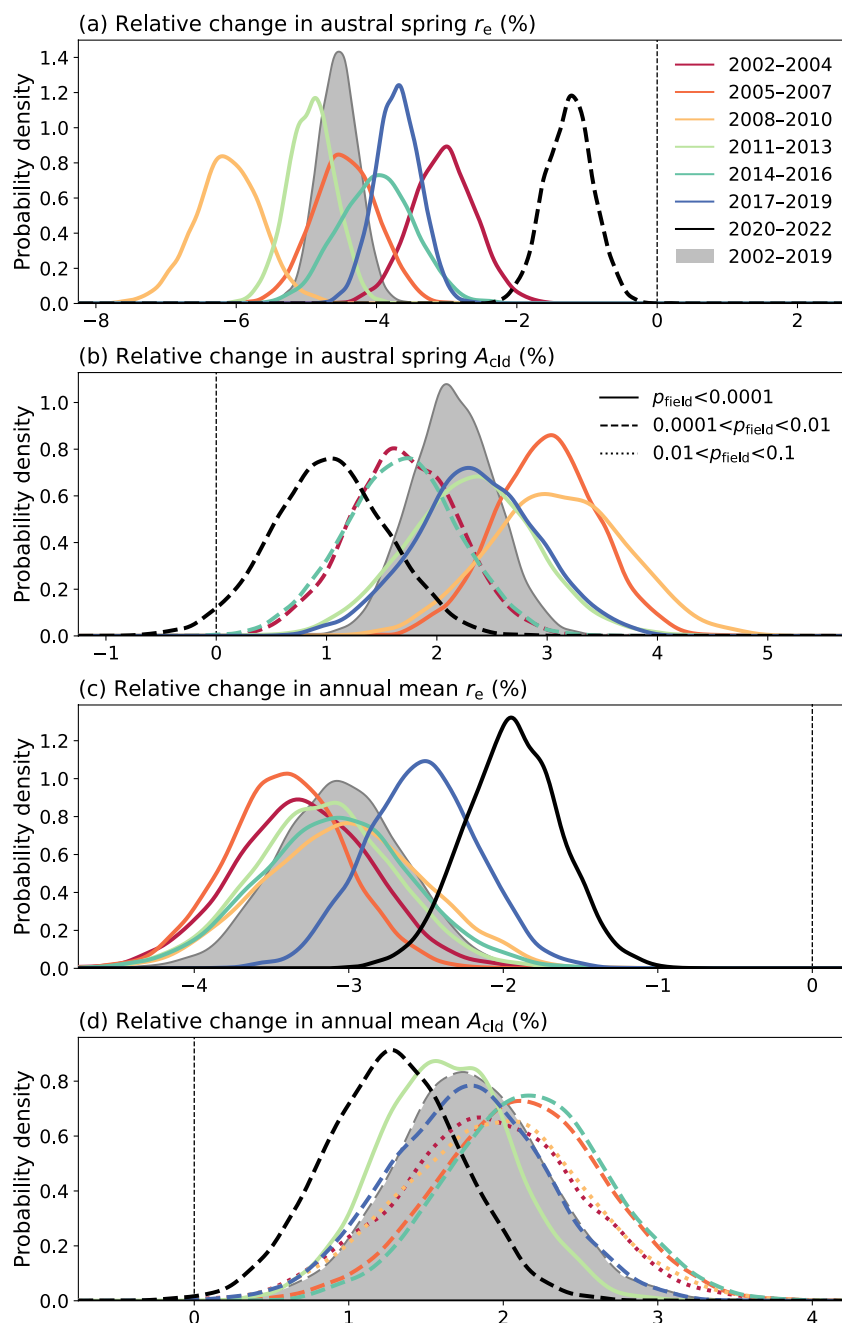
Figure 3. Probability densities (via Gaussian kernel density estimation) for the Ship-NoShip relative differences within the core shipping
corridor for austral spring r_e (a), austral spring A_{cld} (b), annual mean r_e (c), and annual mean A_{cld} (d). The 2002–2019 climatology values are
shown as gray shading, the three-year periods prior to the IMO 2020 regulations as colored lines, and the 2020–2022 period as black lines.
Solid, dashed, and dotted lines indicate decreasing degrees of field significance (p_{field}).

3 Discussion

3.1 Monitoring compliance with IMO regulations

120   Assessing (non)compliance with the IMO 2020 regulations is of critical importance for ensuring that the intended public health benefits are realized. One assessment method is to monitor the sulfur content of the global fuel oil supply. According to data supplied to the IMO MEPC, ~80% of the global fuel oil supply by mass consisted of fuels with sulfur mass contents exceeding 0.5% prior to 2020, whereas only ~20% does since (IMO, 2020, 2021, 2022, 2023). This raw percentage understates compliance, as a "carriage ban" forbids ships from carrying the remaining noncompliant fuel oil unless they have scrubbers

125 installed (IMO, 2018). Geophysical monitoring via cloud changes, as has been shown in Yuan et al. (2022) and Watson-Parris et al. (2022) for ship track occurrence and here for large-scale cloud microphysical properties, offers an independent check that can increase confidence that there has been substantial compliance with the IMO 2020 regulations. As our improving of the cloud effects from shipping aerosol improves, it may become possible to assess regional differences in compliance or even compliance for individual ships with geophysical monitoring.

130   Given the clear detection of cloud microphysical changes in austral spring after the IMO 2020 regulations went into effect, it is reasonable to ask whether advanced statistical methods are necessary for evaluating (some level of) compliance or if simple time series [e.g., Fig. S5 of Watson-Parris et al. (2022)] would suffice. From the time series of austral spring Ship and NoShip r_e values averaged over the southeastern Atlantic (Fig. 4), it is evident that the shipping effect before 2020–2022 is of similar magnitude to interannual variability in the background values and that the 2020–2022 r_e values are estimated to

135 be the highest on record even before any IMO 2020 effect is considered. As an estimate of what the 2020–2022 observed value would have been under a scenario of complete noncompliance with the sulfur regulations, the average Ship-NoShip difference from the 2002–2019 climatology is applied to the 2020–2022 NoShip value (Noncompliance in Fig. 4). The +0.1 μm difference between the observed (Ship) value and this noncompliance hypothetical is due to compliance with the IMO 2020 regulations. If we had rather based our noncompliance scenario on a persistence forecast of the 2017–2019 value and then observed the

140 value from the "true" noncompliance estimate calculated above, we would erroneously conclude that the IMO 2020 regulations were successfully implemented and led to a +0.3 μm increase in regional r_e. Of course, in this latter scenario, the true value of the difference due to IMO 2020 would have been zero and the apparent effect only an artifact of the changing background. Caution is therefore advised in attempting to interpret time series of large-scale cloud properties without applying a method (like track identification or kriging) that plausibly establishes causality.

145
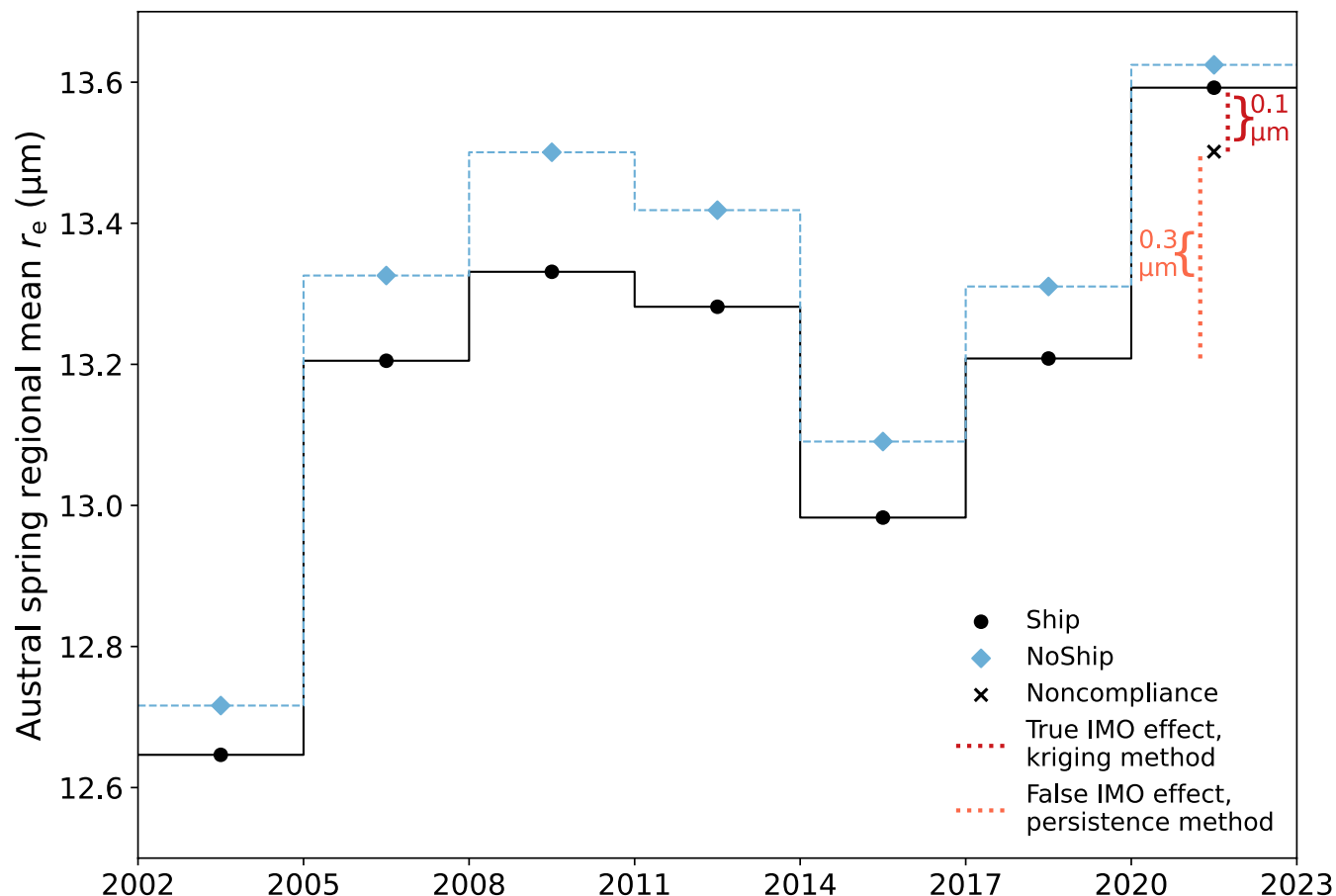
Figure 4. Time series of observed Ship (black circles) and mean NoShip (blue diamonds) values averaged the southeastern Atlantic analysis
domain (18° S to 8° S, 13° W to 8° E). A Noncompliance scenario in which the IMO 2020 regulations were not enforced and the Ship-
NoShip difference in 2020–2022 were the same as for the 2002–2019 climatology is donated as a black "x". The red dotted line denotes the
estimated effect from compliance with the IMO 2020 regulations, calculated as the difference between the observed Ship and hypothetical
Noncompliance value expected for no change in 2020–2022. The orange dotted line denotes the mistakenly determined effect that would
have resulted if the Noncompliance scenario were true and observed but a persistence forecast of 2017–2019 were used as the expectation
value for no change in 2020–2022.

3.2 Radiative forcing implications

Assuming that the Terra-based r_e and A_{cld} perturbations are dominated by the Twomey effect as in D20, it is possible to estimate
160 the instantaneous radiative forcing due to aerosol–cloud interactions (IRF$_{ACI}$; Forster et al., 2021) from the IMO 2020 regulations within the shipping corridor (see Methods in Appendix A). Results are shown in Fig. 5 for the 2002–2019 climatology, 2020–2022, and their difference (interpreted as the effect of the IMO 2020 regulations). The Twomey effect estimates are much better constrained for the calculations using r_e, but those using A_{cld} show consistent results. The IMO 2020 regulations led to an ~2 W m^{-2} IRF$_{ACI}$ within the shipping corridor during austral spring and an ~0.5 W m^{-2} IRF$_{ACI}$ in the annual
165 mean. Taking the ~70% decline in IRF$_{ACI}$ from the austral spring r_e values as an upper bound and applying it to the -0.1 to -0.6 W m^{-2} range of forcing due to shipping emissions from global models (Capaldo et al., 1999; Lauer et al., 2007; Peters et al., 2013; Righi et al., 2011; Sofiev et al., 2018), global forcing values of $O(0.1$ W m$^{-2})$ and up to +0.4 W m^{-2} due to the IMO 2020 regulations are plausible.

170
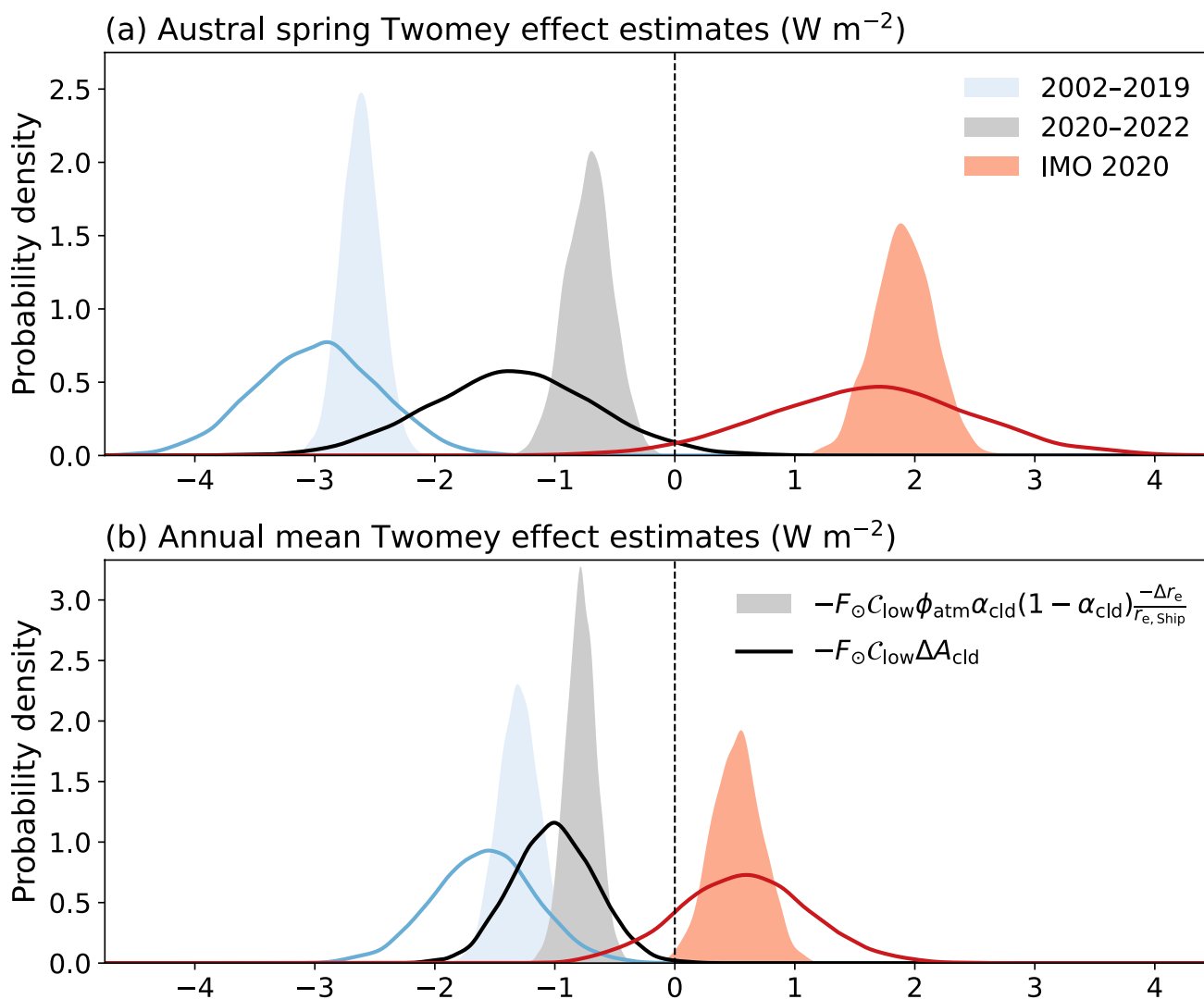
Figure 5. Probability densities (via Gaussian kernel density estimation) of IRF$_{ACI}$ for austral spring (a) and the annual mean (b) over the core shipping corridor calculated using the changes in r_e (shading) and A_{cld} (lines) for the 2002–2019 climatology (blue) and 2020–2022 period (black) due to the presence of the shipping corridor and as the 2020–2022 minus climatology difference as an estimate of the effect due to implementation of the IMO 2020 regulations (red).

4 Conclusions

There is a detectable change in large-scale cloud microphysical properties and evidence supporting a decrease in cloud brightness within the major southeastern Atlantic shipping corridor after implementation of the IMO 2020 fuel sulfur regulations, resulting in a positive IRF$_{ACI}$ within the corridor of $O(1$ W m$^{-2})$. Although this study did not address potential
185 changes in cloud adjustments from the IMO 2020 regulations, this will be an important area of future work, especially as the fuel regulations are expected not only to decrease overall aerosol numbers but also shift them toward smaller sizes and sootier composition (Ault et al., 2010; Lack et al., 2011; Seppälä et al., 2021).

Appendix A: Methods

Data

190 All cloud, radiation, and meteorological data in this work come from the CERES SSF regional 1° x 1° (SSF1deg) monthly product based on the CERES instrument from the Terra satellite (CERES Science Team, 2021, 2023; Loeb et al., 2018; Wielicki et al., 1996). Radiative fluxes are temporally interpolated over the diurnal cycle assuming constant cloud and meteorological properties but varying the solar zenith angle (Doelling et al., 2013). Overcast albedo values are calculated as in Diamond et al. (2020) but with the clear-sky albedo assumed to be 0.1 to avoid issues with missing clear-sky data in the
195 SSF1deg product. The overcast albedo (albedo as seen from space when clouds are present) differs from the cloud albedo (cloud reflectivity) due to the scattering and absorption of sunlight from above-cloud aerosols and gases.

Cloud properties are retrieved from Moderate Resolution Imaging Spectroradiometer (MODIS) measurements using CERES algorithms (CERES Science Team, 2016; Minnis et al., 2011), which have some differences from the standard MODIS products (Platnick et al., 2017). Only daytime cloud retrievals utilizing 3.7 µm channel radiances are used in this work. Low
200 cloud fraction is defined for clouds with cloud top effective pressure values greater than 700 hPa.

Meteorological variables including surface skin temperature (over oceans, the Reynold's sea surface temperature), estimated inversion strength (Wood and Bretherton, 2006), and wind speed are from the NASA Goddard Space Flight Center Global Modeling and Assimilation Office (GMAO) Goddard Earth Observing System (GEOS) version 5.4.1 (CERES Science Team, 2021).

205 Sulfur dioxide (SO$_2$) emissions data from 2010 are from the Emissions Database for Global Atmospheric Research (EDGAR) version 4 (Crippa et al., 2018) and are identical to those used in Diamond et al. (2020). The EDGAR SO$_2$ values are only used for identification of the shipping corridor location.

Shipping corridor identification

For each latitude between 8° S and 18° S, shipping-affected grid boxes are identified as those with the maximum EDGAR SO$_2$
210 emission values between 13° W and 8° E as well as the four grid boxes to the west and two to the east. This represents a

northward and westward expansion of the shipping corridor definition used in Diamond et al. (2020) for their subtropical domain that is intended to better center the microphysical effects. Ship tracking via the automatic identification system (AIS) identifies substantial traffic slightly west of where EDGAR places the maximum SO_2 emissions and there are indications of an additional westward shift in traffic during 2020 (March et al., 2021). As a sensitivity test, the analysis in Fig. 1 was repeated

215   using a shipping corridor mask shifted further west by two degrees, but no notable differences were found. The core shipping corridor area used in Figs. 3 and 5 and Tables S1-2 is defined as the central three grid boxes of the shipping mask for each latitude.

Universal kriging

The universal kriging algorithm mostly follows the implementation of Diamond et al. (2020). Universal kriging is a classic

220   geostatistical method in which estimates of unknown values at some location are informed by nearby observations of the same variable under the assumption that errors around a mean function are spatially correlated as a function of the distance between locations only (stationarity). In our case, counterfactual values for the shipping-affected grid boxes identified are estimated using the values of nearby, non-shipping-affected grid boxes between 8° S and 18° S and 13° W and 8° E. Our mean function takes the form of a multiple linear regression model using as regressors some combination of the surface skin temperature

225   (SST), estimated inversion strength (EIS), and wind speed (WS) from the SSF1deg auxiliary data and latitude (lat), longitude (lon), and their squares (lat^2, lon^2) and product (lat*lon), as determined by whichever combination minimizes the Bayesian information criterion (BIC) to avoid overfitting. Table S1 reports the selected combination of regressors (based on BIC minimization) for each combination of variable (r_e and A_{cld}) and time period. A logit transform is applied to the A_{cld} values before kriging, which was previously found to produce more normally distributed errors around the mean function for bounded

230   fields like albedo and cloud fraction (Diamond et al., 2020). The stationary error term is then estimated by using weighted least squares to fit a parametric (exponential) covariance model to an empirical variogram (a plot of the squared difference between pairs of variables versus their distance). Figures S5-8 show the binned empirical variograms and fitted variograms for austral spring r_e and logit(A_{cld}) and annual mean r_e and logit(A_{cld}), respectively. Using the statistical model provided by the kriging process above, we simulate 5,000 realizations of the NoShip counterfactual for each variable/time period combination.

235   **Statistical significance testing**

Four distinct tests of statistical significance are used in this work, the first three following Diamond et al. (2020). Statistical significance for individual shipping-affected grid boxes is assessed as whether the observed Ship value exceeds the 97.5[th] percentile or falls below the 2.5[th] percentile of the distribution obtained via kriging for the counterfactual NoShip value for that grid box.

240   Field significance is assessed by determining whether the number of individually significant grid boxes calculated above is extreme as compared to that which could occur by chance; p-values are calculated as the fraction of the 5,000 NoShip simulations that would have a number of individually significant grid boxes greater than or equal to the factual case and are

adjusted for multiple testing using a Benjamini-Hochberg adjustment to control the false discovery rate (Benjamini and Hochberg, 1995; Ventura et al., 2004). If none of the 5,000 NoShip simulations would produce a number of individually significant grid boxes as or more extreme than the Ship field, the p-value is reported as <0.0001 instead of zero in Table S1.

The range of Ship-NoShip values generated from the 5,000 simulated NoShip fields is used to assess if the magnitude of effects within the core shipping corridor area are statistically distinct from zero at 95% confidence (Table S1).

Finally, a new test for "detectability" at different confidence interval thresholds is presented in Table S2 and based on the range of possible ratios of 2020–2022 over climatological relative Ship-NoShip values from the 5,000 simulated NoShip fields. We adopt significance at 95% confidence or greater as distinguishing between "detection" for the r_e changes versus "evidence" short of detection for the A_{cld} changes.

Twomey effect calculations

For the r_e perturbations, IRF$_{ACI}$ is estimated as: $-F_\odot C_{low} \phi_{atm} \alpha_{cld}(1 - \alpha_{cld})(-\Delta r_e/r_{e,Ship})$, where $F_\odot$ is the insolation, C_{low} is the low cloud fraction, ϕ_{atm} is a transfer function between changes in overcast and cloud albedo (Diamond et al., 2020; Wood, 2021), and α_{cld} is the cloud albedo. Based on the values in D20, ϕ_{atm} is estimated as 0.6 and α_{cld} as 0.5. For the A_{cld} perturbations, IRF$_{ACI}$ is estimated as: $-F_\odot C_{low} \Delta A_{cld}$.

Code availability

Code for processing the data and recreating the analyses in this work is available from GitHub (https://github.com/michael-s-diamond/IMO2020, last accessed 10 May 2023). The universal kriging algorithm is implemented in R (R Core Team, 2014) using the geoR package (Ribeiro and Diggle, 2018). Other analyses are performed in Python using the numpy (Harris et al., 2020), cartopy (Met Office, 2010-2015), matplotlib (Hunter, 2007), scipy (Virtanen et al., 2020), statsmodels (https://github.com/statsmodels/statsmodels, last accessed 10 May 2023) and xarray (Hoyer and Hamman, 2017) packages.

Data availability

SSF1deg data (CERES Science Team, 2023) are available from the NASA Langley Research Center CERES ordering tool (https://ceres.larc.nasa.gov/data/, last accessed 14 April 2023). EDGAR data (European Commission Joint Research Centre, 2018) are available from the European Commission Joint Research Centre Data Catalogue (https://doi.org/10.2904/JRC_DATASET_EDGAR, last accessed 10 May 2023). Processed data used in this work (Diamond, 2023) are available in a Zenodo repository (https://doi.org/10.5281/zenodo.7864530, last accessed 10 May 2023).

Competing interests

The author declares that they have no conflict of interest.

Acknowledgements

This work was supported with startup funds from Florida State University. Hannah M. Director merits continued gratitude for her contributions to the original code base and analysis methods. Discussion with Leon Simons provided the impetus for attempting to detect a signal with only three years of post-2020 data.

275 **References**

Albrecht, B. A.: Aerosols, Cloud Microphysics, and Fractional Cloudiness, Science, 245, 1227-1230, 10.1126/science.245.4923.1227, 1989.

Ault, A. P., Gaston, C. J., Wang, Y., Dominguez, G., Thiemens, M. H., and Prather, K. A.: Characterization of the Single Particle Mixing State of Individual Ship Plume Events Measured at the Port of Los Angeles, Environmental Science & Technology, 44, 1954-1961, 10.1021/es902985h, 2010.

280 Benjamini, Y., and Hochberg, Y.: Controlling the False Discovery Rate: A Practical and Powerful Approach to Multiple Testing, Journal of the Royal Statistical Society. Series B (Methodological), 57, 289-300, 1995.

Capaldo, K., Corbett, J. J., Kasibhatla, P., Fischbeck, P., and Pandis, S. N.: Effects of ship emissions on sulphur cycling and radiative climate forcing over the ocean, Nature, 400, 743-746, 10.1038/23438, 1999.

CERES Science Team: CERES_SSF_Terra-Aqua_Edition4A Data Quality Summary, NASA Langley Research Center, Langley, VA, 2016.

285 CERES Science Team: CERES_SSF1deg-Hour/Day/Month_Ed4A Data Quality Summary Version 1, NASA Langley Research Center, Langley, VA, 2021.

CERES Science Team: Hampton, VA, USA: NASA Atmospheric Science Data Center (ASDC), Accessed 14 April 2023, doi:10.5067/Terra/CERES/SSF1DegMonth_L3.004A. 2023.

Chen, Y.-C., Christensen, M. W., Xue, L., Sorooshian, A., Stephens, G. L., Rasmussen, R. M., and Seinfeld, J. H.: Occurrence of lower 290 cloud albedo in ship tracks, Atmospheric Chemistry and Physics, 12, 8223-8235, 10.5194/acp-12-8223-2012, 2012.

Christensen, M. W., Gettelman, A., Cermak, J., Dagan, G., Diamond, M., Douglas, A., Feingold, G., Glassmeier, F., Goren, T., Grosvenor, D. P., Gryspeerdt, E., Kahn, R., Li, Z., Ma, P. L., Malavelle, F., McCoy, I. L., McCoy, D. T., McFarquhar, G., Mülmenstädt, J., Pal, S., Possner, A., Povey, A., Quaas, J., Rosenfeld, D., Schmidt, A., Schrödner, R., Sorooshian, A., Stier, P., Toll, V., Watson-Parris, D., Wood, R., Yang, M., and Yuan, T.: Opportunistic experiments to constrain aerosol effective radiative forcing, Atmos. Chem. Phys., 22, 641-674, 295 10.5194/acp-22-641-2022, 2022.

Coakley, J. A., and Walsh, C. D.: Limits to the Aerosol Indirect Radiative Effect Derived from Observations of Ship Tracks, Journal of the Atmospheric Sciences, 59, 668-680, 10.1175/1520-0469(2002)059<0668:Lttair>2.0.Co;2, 2002.

Conover, J. H.: Anomalous Cloud Lines, Journal of the Atmospheric Sciences, 23, 778-785, 10.1175/1520-0469(1966)023<0778:Acl>2.0.Co;2, 1966.

300 Crippa, M., Guizzardi, D., Muntean, M., Schaaf, E., Dentener, F., van Aardenne, J. A., Monni, S., Doering, U., Olivier, J. G. J., Pagliari, V., and Janssens-Maenhout, G.: Gridded emissions of air pollutants for the period 1970–2012 within EDGAR v4.3.2, Earth System Science Data, 10, 1987-2013, 10.5194/essd-10-1987-2018, 2018.

Diamond, M. S., Director, H. M., Eastman, R., Possner, A., and Wood, R.: Substantial Cloud Brightening from Shipping in Subtropical Low Clouds, AGU Advances, 1, e2019AV000111, 10.1029/2019av000111, 2020.

305 Diamond, M. S.: Data for "Detection of large-scale cloud microphysical changes and evidence for decreasing cloud brightness within a major shipping corridor after implementation of the International Maritime Organization 2020 fuel sulfur regulations" (Version 20230426) [Data set]. Zenodo, 10.5281/zenodo.7864530. 2023.

Doelling, D. R., Loeb, N. G., Keyes, D. F., Nordeen, M. L., Morstad, D., Nguyen, C., Wielicki, B. A., Young, D. F., and Sun, M.: Geostationary Enhanced Temporal Interpolation for CERES Flux Products, Journal of Atmospheric and Oceanic Technology, 30, 1072- 310 1090, 10.1175/jtech-d-12-00136.1, 2013.

European Commission Joint Research Centre: Emissions Database for Global Atmospheric Research [Data set]. Joint Research Centre Data Catalogue, 10.2904/JRC_DATASET_EDGAR. 2018.

Forster, P., T. Storelvmo, K. Armour, W. Collins, J.-L. Dufresne, D. Frame, D.J. Lunt, T. Mauritsen, M.D. Palmer, M. Watanabe, M. Wild, and Zhang, H.: The Earth's Energy Budget, Climate Feedbacks, and Climate Sensitivity, in: Climate Change 2021: The Physical Science 315 Basis. Contribution of Working Group I to the Sixth Assessment Report of the Intergovernmental Panel on Climate Change, Cambridge University Press, Cambridge, United Kingdom and New York, NY, USA, 923–1054, 2021.

Goren, T., and Rosenfeld, D.: Satellite observations of ship emission induced transitions from broken to closed cell marine stratocumulus over large areas, Journal of Geophysical Research: Atmospheres, 117, D17206, 10.1029/2012jd017981, 2012.

Gryspeerdt, E., Smith, T. W. P., O'Keeffe, E., Christensen, M. W., and Goldsworth, F. W.: The Impact of Ship Emission Controls Recorded by Cloud Properties, Geophysical Research Letters, 46, 12547– 12555, 10.1029/2019gl084700, 2019.

Harris, C. R., Millman, K. J., van der Walt, S. J., Gommers, R., Virtanen, P., Cournapeau, D., Wieser, E., Taylor, J., Berg, S., Smith, N. J., Kern, R., Picus, M., Hoyer, S., van Kerkwijk, M. H., Brett, M., Haldane, A., Del Rio, J. F., Wiebe, M., Peterson, P., Gerard-Marchant, P., Sheppard, K., Reddy, T., Weckesser, W., Abbasi, H., Gohlke, C., and Oliphant, T. E.: Array programming with NumPy, Nature, 585, 357-362, 10.1038/s41586-020-2649-2, 2020.

Hoyer, S., and Hamman, J. J.: xarray: N-D labeled Arrays and Datasets in Python, Journal of Open Research Software, 5, 10.5334/jors.148, 2017.

Hunter, J. D.: Matplotlib: A 2D Graphics Environment, Computing in Science & Engineering, 9, 90-95, 10.1109/MCSE.2007.55, 2007.

IMO: RESOLUTION MEPC.305(73): AMENDMENTS TO THE ANNEX OF THE PROTOCOL OF 1997 TO AMEND THE INTERNATIONAL CONVENTION FOR THE PREVENTION OF POLLUTION FROM SHIPS, 1973, AS MODIFIED BY THE PROTOCOL OF 1978 RELATING THERETO. London, UK, 2018.

IMO: RESOLUTION MEPC.320(74): 2019 GUIDELINES FOR CONSISTENT IMPLEMENTATION OF THE 0.50% SULPHUR LIMIT UNDER MARPOL ANNEX VI. London, UK, 2019.

IMO: MEPC 75/5/9: Sulphur monitoring for 2019, London, UK, 2020.

IMO: MEPC 76/5/2: Relevant information reported to IMO related to the entry into force of the global 0.50% sulphur limit (IMO2020) and outcomes of the sulphur monitoring programme for 2020, London, UK, 2021.

IMO: MEPC 78/INF.4: Relevant information reported to IMO related to the implementation of the global 0.50% sulphur limit (IMO2020) and outcomes of the sulphur monitoring for 2021, London, UK, 2022.

IMO: MEPC 80/INF.4: Relevant information reported to IMO related to the entry into force of the global 0.50% sulphur limit (IMO 2020) and outcomes of the sulphur monitoring for 2022, London, UK, 2023.

Lack, D. A., Cappa, C. D., Langridge, J., Bahreini, R., Buffaloe, G., Brock, C., Cerully, K., Coffman, D., Hayden, K., Holloway, J., Lerner, B., Massoli, P., Li, S. M., McLaren, R., Middlebrook, A. M., Moore, R., Nenes, A., Nuaaman, I., Onasch, T. B., Peischl, J., Perring, A., Quinn, P. K., Ryerson, T., Schwartz, J. P., Spackman, R., Wofsy, S. C., Worsnop, D., Xiang, B., and Williams, E.: Impact of fuel quality regulation and speed reductions on shipping emissions: implications for climate and air quality, Environ Sci Technol, 45, 9052-9060, 10.1021/es2013424, 2011.

Lauer, A., Eyring, V., Hendricks, J., Jöckel, P., and Lohmann, U.: Global model simulations of the impact of ocean-going ships on aerosols, clouds, and the radiation budget, Atmospheric Chemistry and Physics, 7, 5061-5079, 10.5194/acp-7-5061-2007, 2007.

Loeb, N. G., Su, W., Doelling, D. R., Wong, T., Minnis, P., Thomas, S., and Miller, W. F.: Earth's Top-of-Atmosphere Radiation Budget, in: Comprehensive Remote Sensing, 67-84, 2018.

Manshausen, P., Watson-Parris, D., Christensen, M. W., Jalkanen, J.-P., and Stier, P.: Invisible ship tracks show large cloud sensitivity to aerosol, Nature, 610, 101-106, 10.1038/s41586-022-05122-0, 2022.

March, D., Metcalfe, K., Tintore, J., and Godley, B. J.: Tracking the global reduction of marine traffic during the COVID-19 pandemic, Nat Commun, 12, 2415, 10.1038/s41467-021-22423-6, 2021.

Met Office: Cartopy: a cartographic python library with a matplotlib interface. Met Office (Ed.), Exeter, Devon, 2010-2015.

Minnis, P., Sun-Mack, S., Young, D. F., Heck, P. W., Garber, D. P., Chen, Y., Spangenberg, D. A., Arduini, R. F., Trepte, Q. Z., Smith, W. L., Ayers, J. K., Gibson, S. C., Miller, W. F., Hong, G., Chakrapani, V., Takano, Y., Liou, K.-N., Xie, Y., and Yang, P.: CERES Edition-2 Cloud Property Retrievals Using TRMM VIRS and Terra and Aqua MODIS Data—Part I: Algorithms, IEEE Transactions on Geoscience and Remote Sensing, 49, 4374-4400, 10.1109/tgrs.2011.2144601, 2011.

Partanen, A. I., Laakso, A., Schmidt, A., Kokkola, H., Kuokkanen, T., Pietikäinen, J. P., Kerminen, V. M., Lehtinen, K. E. J., Laakso, L., and Korhonen, H.: Climate and air quality trade-offs in altering ship fuel sulfur content, Atmospheric Chemistry and Physics, 13, 12059-12071, 10.5194/acp-13-12059-2013, 2013.

Peters, K., Quaas, J., and Graßl, H.: A search for large-scale effects of ship emissions on clouds and radiation in satellite data, Journal of Geophysical Research: Atmospheres, 116, D24205, 10.1029/2011jd016531, 2011.

Peters, K., Stier, P., Quaas, J., and Graßl, H.: Corrigendum to "Aerosol indirect effects from shipping emissions: sensitivity studies with the global aerosol-climate model ECHAM-HAM" published in Atmos. Chem. Phys., 12, 5985–6007, 2012, Atmos. Chem. Phys., 13, 6429-6430, 10.5194/acp-13-6429-2013, 2013.

Platnick, S., Meyer, K. G., King, M. D., Wind, G., Amarasinghe, N., Marchant, B., Arnold, G. T., Zhang, Z., Hubanks, P. A., Holz, R. E., Yang, P., Ridgway, W. L., and Riedi, J.: The MODIS cloud optical and microphysical products: Collection 6 updates and examples from Terra and Aqua, IEEE Transactions on Geoscience and Remote Sensing, 55, 502-525, 10.1109/TGRS.2016.2610522, 2017.

R Core Team: R: A Language and Environment for Statistical Computing. R Foundation for Statistical Computing, Vienna, Austria, 2014.

geoR: Analysis of Geostatistical Data. R package version 1.7-5.2.1: https://CRAN.R-project.org/package=geoR, 2018.

Righi, M., Klinger, C., Eyring, V., Hendricks, J., Lauer, A., and Petzold, A.: Climate impact of biofuels in shipping: global model studies of the aerosol indirect effect, Environmental Science & Technology, 45, 3519-3525, 10.1021/es1036157, 2011.

Schreier, M., Mannstein, H., Eyring, V., and Bovensmann, H.: Global ship track distribution and radiative forcing from 1 year of AATSR data, Geophysical Research Letters, 34, L17814, 10.1029/2007gl030664, 2007.

375 Seppälä, S. D., Kuula, J., Hyvärinen, A. P., Saarikoski, S., Rönkkö, T., Keskinen, J., Jalkanen, J. P., and Timonen, H.: Effects of marine fuel sulfur restrictions on particle number concentrations and size distributions in ship plumes in the Baltic Sea, Atmos. Chem. Phys., 21, 3215-3234, 10.5194/acp-21-3215-2021, 2021.

Sofiev, M., Winebrake, J. J., Johansson, L., Carr, E. W., Prank, M., Soares, J., Vira, J., Kouznetsov, R., Jalkanen, J. P., and Corbett, J. J.: Cleaner fuels for ships provide public health benefits with climate tradeoffs, Nature Communications, 9, 406, 10.1038/s41467-017-02774-9, 2018.

380 Toll, V., Christensen, M., Quaas, J., and Bellouin, N.: Weak average liquid-cloud-water response to anthropogenic aerosols, Nature, 572, 51-55, 10.1038/s41586-019-1423-9, 2019.

Twomey, S., Howell, H. B., and Wojciechowski, T. A.: Comments on "Anomalous Cloud Lines", Journal of the Atmospheric Sciences, 25, 333-334, 10.1175/1520-0469(1968)025<0333:Cocl>2.0.Co;2, 1968.

385 Twomey, S.: Pollution and the Planetary Albedo, Atmospheric Environment, 8, 1251-1256, 10.1016/0004-6981(74)90004-3, 1974.

Twomey, S.: The Influence of Pollution on the Shortwave Albedo of Clouds, Journal of the Atmospheric Sciences, 34, 1149-1152, 10.1175/1520-0469(1977)034<1149:tiopot>2.0.co;2, 1977.

Ventura, V., Paciorek, C. J., and Risbey, J. S.: Controlling the Proportion of Falsely Rejected Hypotheses when Conducting Multiple Tests with Climatological Data, Journal of Climate, 17, 4343-4356, 10.1175/3199.1, 2004.

390 Virtanen, P., Gommers, R., Oliphant, T. E., Haberland, M., Reddy, T., Cournapeau, D., Burovski, E., Peterson, P., Weckesser, W., Bright, J., van der Walt, S. J., Brett, M., Wilson, J., Millman, K. J., Mayorov, N., Nelson, A. R. J., Jones, E., Kern, R., Larson, E., Carey, C. J., Polat, I., Feng, Y., Moore, E. W., VanderPlas, J., Laxalde, D., Perktold, J., Cimrman, R., Henriksen, I., Quintero, E. A., Harris, C. R., Archibald, A. M., Ribeiro, A. H., Pedregosa, F., van Mulbregt, P., and SciPy, C.: SciPy 1.0: fundamental algorithms for scientific computing in Python, Nat Methods, 17, 261-272, 10.1038/s41592-019-0686-2, 2020.

395 Watson-Parris, D., Christensen, M. W., Laurenson, A., Clewley, D., Gryspeerdt, E., and Stier, P.: Shipping regulations lead to large reduction in cloud perturbations, Proc Natl Acad Sci U S A, 119, e2206885119, 10.1073/pnas.2206885119, 2022.

Wielicki, B. A., Barkstrom, B. R., Harrison, E. F., Lee, R. B., Smith, G. L., and Cooper, J. E.: Clouds and the Earth's Radiant Energy System (CERES): An Earth Observing System Experiment, Bulletin of the American Meteorological Society, 77, 853-868, 10.1175/1520-0477(1996)077<0853:Catere>2.0.Co;2, 1996.

400 Wood, R., and Bretherton, C. S.: On the Relationship between Stratiform Low Cloud Cover and Lower-Tropospheric Stability, Journal of Climate, 19, 6425-6432, 2006.

Wood, R.: Assessing the potential efficacy of marine cloud brightening for cooling Earth using a simple heuristic model, Atmos. Chem. Phys., 21, 14507-14533, 10.5194/acp-21-14507-2021, 2021.

Yuan, T., Wang, C., Song, H., Platnick, S., Meyer, K., and Oreopoulos, L.: Automatically Finding Ship Tracks to Enable Large-Scale 405 Analysis of Aerosol-Cloud Interactions, Geophysical Research Letters, 46, 7726-7733, 10.1029/2019gl083441, 2019.

Yuan, T., Song, H., Wood, R., Wang, C., Oreopoulos, L., Platnick, S. E., von Hippel, S., Meyer, K., Light, S., and Wilcox, E.: Global reduction in ship-tracks from sulfur regulations for shipping fuel, Science Advances, 8, eabn7988, doi:10.1126/sciadv.abn7988, 2022.

Zhang, Y., Eastham, S. D., Lau, A. K. H., Fung, J. C. H., and Selin, N. E.: Global air quality and health impacts of domestic and international shipping, Environmental Research Letters, 16, 10.1088/1748-9326/ac146b, 2021.

410 Zimmerman, D. L., and Stein, M.: Classical Geostatistical Methods, in: Handbook of Spatial Statistics, edited by: A. E. Gelfand, P. J. Diggle, M. Fuentes, and Guttorp, P., 29-44, 2010.